AGU PUBLICATIONS

Water Resources Research

TECHNICAL REPORTS: METHODS

10.1002/2016WR020317

Key Points:
- A vapor intrusion model for simulating 2-D soil-gas concentration profiles in vertically heterogeneous soils is presented
- The output of this new model is in line with published field data
- This new model can replicate 2-D the soil gas concentration profiles simulated by 3-D numerical models

Supporting Information:
- Supporting Information S1

Correspondence to:
Y. Yao,
Yijun_Yao@zju.edu.cn;
I. Verginelli,
verginelli@ing.uniroma2.it

Citation:
Yao, Y., I. Verginelli, and E. M. Suuberg (2017), A two-dimensional analytical model of vapor intrusion involving vertical heterogeneity, *Water Resour. Res.*, *53*, 4499–4513, doi:10.1002/2016WR020317.

Received 21 DEC 2016
Accepted 23 APR 2017
Accepted article online 2 MAY 2017
Published online 22 MAY 2017

A two-dimensional analytical model of vapor intrusion involving vertical heterogeneity

Yijun Yao[1,2,3], Iason Verginelli[4], and Eric M. Suuberg[5]

[1]Key Lab of Environmental Remediation and Ecosystem Health (Ministry of Education), College of Environmental and Resource Sciences, Zhejiang University, Hangzhou, China, [2]Research Center for Air Pollution and Health, Zhejiang University, Hangzhou, China, [3]Institute of Environmental Health, Zhejiang University, Hangzhou, China, [4]Department of Civil Engineering and Computer Science Engineering, University of Rome, Rome, Italy, [5]School of Engineering, Brown University, Providence, Rhode Island, USA

Abstract In this work, we present an analytical chlorinated vapor intrusion (CVI) model that can estimate source-to-indoor air concentration attenuation by simulating two-dimensional (2-D) vapor concentration profile in vertically heterogeneous soils overlying a homogenous vapor source. The analytical solution describing the 2-D soil gas transport was obtained by applying a modified Schwarz-Christoffel mapping method. A partial field validation showed that the developed model provides results (especially in terms of indoor emission rates) in line with the measured data from a case involving a building overlying a layered soil. In further testing, it was found that the new analytical model can very closely replicate the results of three-dimensional (3-D) numerical models at steady state in scenarios involving layered soils overlying homogenous groundwater sources. By contrast, by adopting a two-layer approach (capillary fringe and vadose zone) as employed in the EPA implementation of the Johnson and Ettinger model, the spatially and temporally averaged indoor concentrations in the case of groundwater sources can be higher than the ones estimated by the numerical model up to two orders of magnitude. In short, the model proposed in this work can represent an easy-to-use tool that can simulate the subsurface soil gas concentration in layered soils overlying a homogenous vapor source while keeping the simplicity of an analytical approach that requires much less computational effort.

1. Introduction

In the technical guide of vapor intrusion (VI) released by *U.S. EPA* [2015], mathematical modeling is mentioned as one line of evidence in supporting risk management decisions for VI contaminated sites. In some scenarios, such as brownfield redevelopment cases, mathematical models are particularly useful in estimating reasonable maximum indoor air concentrations for the hypothetical future user, as direct measurements of the concentrations at the point of exposure (e.g., indoor concentration) are not available. To obtain plausible predictions in VI investigations, U.S. EPA suggested that the mathematical model should be calibrated by comparison with measured, site-specific values. To satisfy this, mathematical models need to reasonably represent the complex system and should avoid over-simplification of the realistic field situation.

There have been numerous mathematical models developed to simulate the migration of subsurface volatile chemicals into the enclosed space of the concerned building [*Johnson and Ettinger*, 1991; *Fischer et al.*, 1996; *Turczyowicz and Robinson*, 2001; *Olson and Corsi*, 2002; *Hers et al.*, 2002; *Abreu and Johnson*, 2005; *Mills et al.*, 2007; *Pennell et al.*, 2009; *Yu et al.*, 2009; *Bozkurt et al.*, 2009; *Provoost et al.*, 2009; *Atteia and Hohener*, 2010; *Yao et al.*, 2011; *Abreu and Schuver*, 2012; *Picone et al.*, 2012; *Yao et al.*, 2012; *Shen et al.*, 2012; *Johnston and Gibson*, 2013]. For VI of chlorinated chemicals (CVI), the most commonly used model is the *Johnson and Ettinger* [1991] model (JEM), which is based on one-dimensional (1-D) mass conservation among the contaminant diffusive flux from the vapor source, entry rate into the enclosed space and exchange rate with ambient air [*U.S. EPA*, 2004]. This highly idealized assumption overlooks the contaminant flux escaping to atmosphere through the open ground surface surrounding the concerned building, as 1-D model cannot capture the variation in contaminant concentrations parallel to the ground surface [*Yao et al.*, 2011]. To overcome this, *Shen et al.* [2014] proposed an analytical model that can generate two-dimensional (2-D) subfoundation soil gas concentration profiles. Nonetheless, this model does not work for scenarios with

heterogeneous soil properties, which could be caused by layering, vertical variation of moisture content due the capillary-fringe effect or other spatial variabilities of soil [*Zhang et al*., 2015; *Man et al*., 2016]. *Abreu and Johnson* [2005] developed a three-dimensional (3-D) model (AJM) that is capable of simulating complex systems involving layering, transient effects, and oxygen-limited biodegradation. However, as a numerical model, AJM requires considerable computational efforts and training, both of which limit its use as a common screening tool with a public access to usual investigators.

In this study, we are going to present an analytical model that can simulate 2-D subsurface soil gas concentration profiles and indoor air concentrations in CVI scenarios involving vertically heterogeneous soils overlying a homogenous vapor source. After introducing the model development, we will compare the predicted soil gas concentration profiles of the new 2-D model with measured field data and those of 3-D numerical models for scenarios involving layering and vertical variation of moisture content caused by groundwater sources, for a partial validation. At last, we will perform a comparison among numerical simulations, predictions by the EPA implementation of JEM and this new model by examining the responses of the source-to-indoor air attenuation factor (α) to soil type and source depth.

2. Method

2.1. Homogenous Soil

In the absence of advection and biodegradation, the governing equation of soil gas transport with the assumption of steady state diffusion in a two-dimensional (x,y) homogenous soil domain can be written as a Laplace equation:

$$\frac{\partial^2 c}{\partial x^2}+\frac{\partial^2 c}{\partial y^2}=0 \tag{1}$$

For a slab-on grade scenario, an analytical solution of equation (1) was obtained by *Shen et al*. [2014] by employing the Schwarz-Christoffel mapping method with the boundary conditions shown in Figure 1a. In particular, *Shen et al*. [2014] assumed that: the soil is homogenous, the source is uniformly distributed beneath the whole modeling domain ($c=c_s$ *at* $y=0$); the concentration at the open ground surface is constant ($c=c_{atm}$ *at* $y=Ls$ in the segment ab shown in Figure 1a); the bottom of the building foundations (segment bc in Figure 1a) is impermeable to soil gas flow ($\partial c/\partial y=0$); there is no lateral flux through the building center ($\partial c/\partial x=0$ at segment cd in Figure 1a) due to symmetry.

Under these conditions, the relation between the vapor concentration c and its contour coordinates (x,y) can be written as [*Shen et al*., 2014]:

$$\Omega\cos\left(\frac{\pi y}{L_s}\right)\cosh\left(\frac{\pi x}{L_s}\right)-\Omega+1=\cos\left(\pi w\right)\sqrt{\left(\frac{\Omega\,\sin\left(\frac{\pi y}{L_s}\right)\sinh\left(\frac{\pi x}{L_s}\right)}{\sin\left(\pi w\right)}\right)^2+1} \tag{2}$$

with

$$\Omega=\frac{4\exp\left(\frac{\pi L_f}{L_s}\right)}{\left(\exp\left(\frac{\pi L_f}{L_s}\right)+1\right)^2} \tag{3}$$

$$w=\frac{c_s-c}{c_s-c_{atm}} \tag{4}$$

where L_f [L] is the half-width of the building, L_s [L] the source to building foundations vertical distance, c_s [M/L^3] the source vapor concentration, and c_{atm} [M/L^3] the concentration of vapors in atmosphere. Readers interested to more details about the derivation of equation (2) are directed to *Shen et al*. [2014].

Yao et al. [2016] and *Verginelli et al*. [2016] derived an explicit analytical solution of equation (2) for biodegradable compounds (i.e., petroleum hydrocarbons) that allows to estimate the spatial coordinate, e.g., $x(y)$, for a given concentration:

$$x(y)=\begin{cases}\frac{L_s}{\pi}\text{arccosh}\left(\frac{a}{b}+\sqrt{\frac{a^2}{b^2}-\frac{c}{b}}\right) & w\le\frac{1}{2}\ \text{and}\ b\le 0\ \text{or}\ w>\frac{1}{2}\ \text{and}\ b>0\\ \frac{L_s}{\pi}\text{arccosh}\left(\frac{a}{b}-\sqrt{\frac{a^2}{b^2}-\frac{c}{b}}\right) & w>\frac{1}{2}\ \text{and}\ b\le 0\ \text{or}\ w\le\frac{1}{2}\ \text{and}\ b>0\end{cases} \tag{5a}$$

$$a=\frac{(\Omega-1)\Omega\cos\left(\frac{\pi y}{L_s}\right)}{\cos^2(\pi w)} \tag{6a}$$

$$b=\Omega^2\left(\left(\frac{\cos\left(\frac{\pi y}{L_s}\right)}{\cos(\pi w)}\right)^2-\left(\frac{\sin\left(\frac{\pi y}{L_s}\right)}{\sin(\pi w)}\right)^2\right) \tag{6b}$$

$$c=\left(\frac{\Omega-1}{\cos(\pi w)}\right)^2-1+\left(\frac{\Omega\sin\left(\frac{\pi y}{L_s}\right)}{\sin(\pi w)}\right)^2 \tag{6c}$$

For scenarios involving building foundation depth into the soil ($d_f > 0$), the previous equations can still be used but in this case the concentration at the foundation depth beyond the building edge (segment ba in Figure 1b) is assumed to be equal to $c=c_f$. In practice, equations (5) and (6) can be used by replacing the parameter w with:

$$w_{basement}=\frac{c_s-c}{c_s-c_f} \tag{7}$$

For a diffusion-dominated transport, the concentration at the foundation depth beyond the foundation edge (c_f [M/L^3]) to be used in equation (7) can be calculated as follows [*Shen et al.*, 2014]:

$$c_f(y=L_s)=c_{atm}+(c_s-c_{atm})\left(\frac{d_f}{L_s+d_f}\right) \tag{8}$$

where d_f [L] is the building foundation depth below ground surface.

2.2. Vertically Heterogeneous Soil

In the presence of vertical heterogeneity resulting from geological barrier or capillary fringe effects, the diffusion of vapors in the subsurface will be influenced by the vertical moisture profile. The diffusion of vapors can be described with the following equation [*Millington and Quirk*, 1961]:

$$D_e=D_g\frac{\theta_g^{10/3}}{\theta_t^2}+D_w\frac{\theta_w^{10/3}}{K_H\theta_t^2} \tag{9}$$

where D_e [L^2/T], D_g [L^2/T], and D_w [L^2/T] are the diffusivity of the contaminant in porous media, air and water, respectively. θ_t [L^3/L^3], θ_g [L^3/L^3], and θ_w [L^3/L^3] are the total porosity, air-filled porosity and water-filled porosity, respectively, and K_H [L^3/L^3] the dimensionless Henry's constant.

To calculate the overall diffusion coefficient across a layered soil of thickness L_s [L], the following equation can be used [*Johnson and Ettinger*, 1991]:

$$D_{e,tot}=\frac{L_s}{\int_0^{L_s}\frac{1}{D_e(y)}dy} \tag{10}$$

where $D_e(y)$ [L^2/T] is the diffusion coefficient calculated with equation (9) at a given depth y as a function of the total porosity, air-filled porosity, and water-filled porosity at that position.

Equation (10) can be discretized in a system of n layers as:

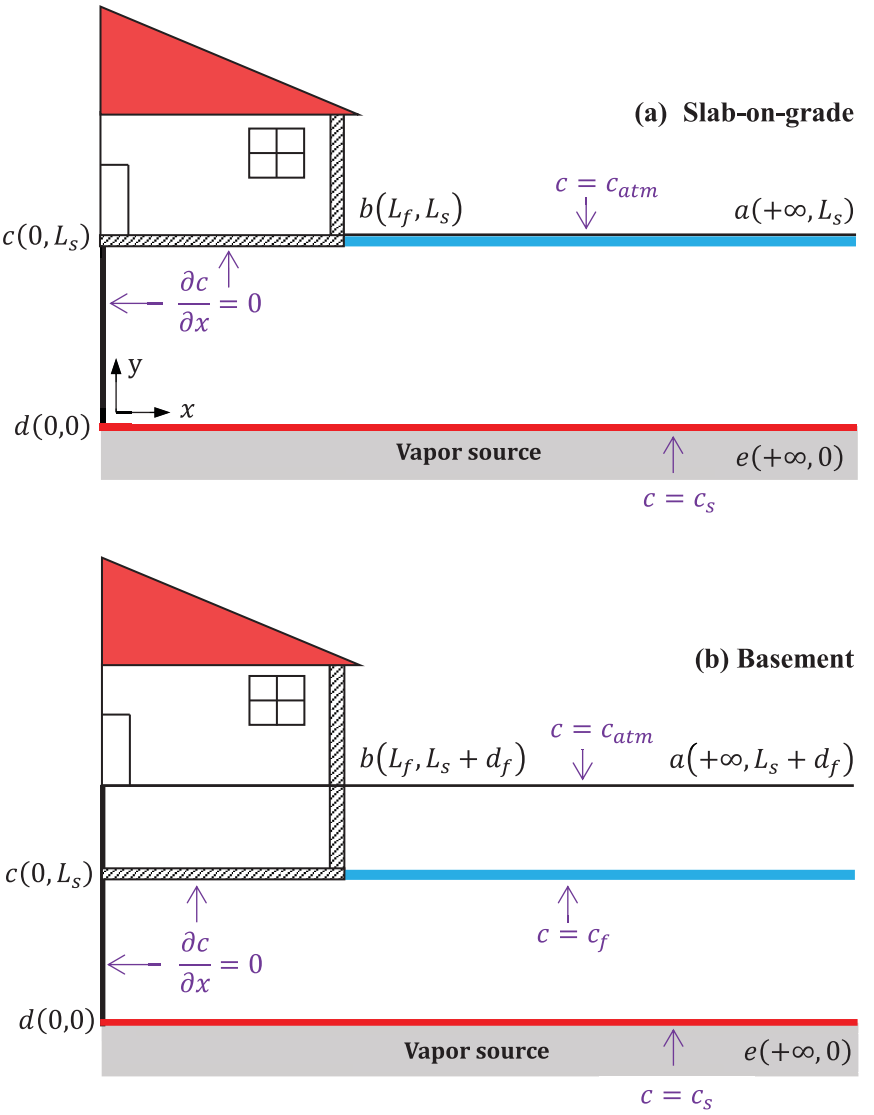

Figure 1. Model domain and boundary conditions employed for (a) slab-on-grade and (b) basement scenario.

$$D_{e,tot} = \frac{L_s}{\sum_{i=0}^{n} \frac{d_i}{D_e(i)}} \tag{11}$$

where d_i [L] and $D_e(i)$ [L^2/T] are the thickness and the diffusion coefficient of the ith layer.

In practice, the introduction of an overall diffusion coefficient as shown in equation (10) allows to transform a layered system in an equivalent homogenous system. From equation (10), it is possible to adapt the model described in the previous section for homogenous soil to an equivalent model that simulates the vapor concentration profiles through a vertically heterogeneous soil. This can be easily done, by rearranging equation (10) to estimate an equivalent source depth as a function of the overall diffusion coefficient:

$$L_{s,eq} = D_e(L_s) \int_0^{L_s} \frac{1}{D_e(y)} dy \tag{12}$$

In the same way, for a given depth y, from equation (10) we can introduce:

$$y_{eq}=D_e(y)\int_0^y \frac{1}{D_e(y)}dy \tag{13}$$

Hence, by substituting equations (12) and (13) into equations (5) and (6), the relation between the vapor concentration c and its contour coordinates (x,y) can be written for a layered system as:

$$x(y)=\begin{cases} \frac{L_{s,eq}}{\pi}\text{arccosh}\left(\frac{a}{b}+\sqrt{\frac{a^2}{b^2}-\frac{c}{b}}\right) & w\le\frac{1}{2}\ \ and\ \ b\le 0\ \ or\ \ w>\frac{1}{2}\ \ and\ \ b>0 \quad (14a)\\ \frac{L_{s,eq}}{\pi}\text{arccosh}\left(\frac{a}{b}-\sqrt{\frac{a^2}{b^2}-\frac{c}{b}}\right) & w>\frac{1}{2}\ \ and\ \ b\le 0\ \ or\ \ w\le\frac{1}{2}\ \ and\ \ b>0 \quad (14b)\end{cases}$$

where

$$\begin{cases} a=\dfrac{(\Omega_{eq}-1)\Omega_{eq}\cos\left(\frac{\pi y_{eq}}{L_{s,eq}}\right)}{\cos^2(\pi w)} & (15a)\\ b=\Omega_{eq}{}^2\left(\left(\dfrac{\cos\left(\frac{\pi y_{eq}}{L_{s,eq}}\right)}{\cos(\pi w)}\right)^2-\left(\dfrac{\sin\left(\frac{\pi y_{eq}}{L_{s,eq}}\right)}{\sin(\pi w)}\right)^2\right) & (15b)\\ c=\left(\dfrac{\Omega_{eq}-1}{\cos(\pi w)}\right)^2-1+\left(\dfrac{\Omega_{eq}\sin\left(\frac{\pi y_{eq}}{L_{s,eq}}\right)}{\sin(\pi w)}\right)^2 & (15c)\end{cases}$$

with

$$\Omega_{eq}=\frac{4\exp\left(\frac{\pi L_f}{L_{s,eq}}\right)}{\left(\exp\left(\frac{\pi L_f}{L_{s,eq}}\right)+1\right)^2} \tag{16}$$

The parameter w in equation (15) can be calculated with equation (4) or equation (7) for a slab-on-grade or a basement scenario, respectively. For a basement scenario, the concentration at the foundation depth beyond the building edge (c_f) to be used in equation (7) for a layered soil can be calculated as:

$$c_f=c_{atm}+(c_s-c_{atm})\left(\frac{\int_y^{L_s+d_f}\frac{dy}{D_e(y)}}{\int_0^{L_s+d_f}\frac{dy}{D_e(y)}}\right) \tag{17}$$

2.3. The Calculation of Indoor Air Concentration

In this study, we provide two methods to estimate the indoor air concentration. The first is the traditional "continuous stirred tank reactor" method as employed in JEM and AJM [*Johnson and Ettinger*, 1991; *Abreu and Johnson*, 2005]. This method is generally used to calculate the spatially and temporally averaged indoor air concentration, by employing the subslab concentration at a perimeter crack, soil gas entry rate and indoor air exchange rate.

The subslab concentration of vapors $c(x,L_s)$ in a layered soil can be estimated from equations (2) and (10) as:

$$c(x,L_s)=c_s-\left(\frac{c_s-c_i}{\pi}\right)\text{arccos}\left(-\Omega_{eq}\cosh\left(\frac{\pi x}{L_{s,eq}}\right)-\Omega_{eq}+1\right) \tag{18}$$

where

$$c_i = \begin{cases} c_{atm} \ \textit{for slab on grade cases} & (19a) \\ c_f \ \textit{for basement cases} & (19b) \end{cases}$$

In most CVI scenarios, advection is believed to dominate the soil gas transport through the foundation cracks [*Robinson and Sextro*, 1997; *McHugh et al*., 2012]. However, in a few cases (e.g., very low effective diffusivity of soil gas due to high moisture content), advection would be weakened and diffusion may play a significant role. To maintain a mass balance between the contaminant flux toward the crack and the flux though the crack, the subslab crack concentration would be lower than that at the surrounding of the crack, and could be estimated using the following flux balance:

$$\frac{c(x_{ck}, L_s)}{r} \cdot D_e(L_s) \cdot \pi \cdot r = \frac{c_{ck}}{L_{ck}} \cdot D_g \cdot w_{ck} \tag{20}$$

where x_{ck} [L] is the x coordinate of crack location, r [L] the radius out of which the crack would not affect the soil gas concentration, c_{ck} [M/L^3] the subslab crack concentration, L_{ck} [L] the thickness of the foundation, and w_{ck} [L] the width of the crack. Equation (20) can be written as:

$$c_{ck} = \frac{\pi D_e(L_s) L_{ck}}{D_g w_{ck}} c(x_{ck}, L_s) \tag{21}$$

In practice, we can use:

$$c_{ck} = \min\left(1, \ \frac{\pi D_e(L_s) L_{ck}}{D_g w_{ck}}\right) \cdot c(x_{ck}, L_s) \tag{22}$$

Next, the indoor concentration, c_{in} [M/L^3], can be calculated as a function of c_{ck}, with the analytical solution extrapolated from JEM [*Johnson and Ettinger*, 1991]:

$$c_{in} = c_{ck}\left(\frac{R_{mix}}{R_{crack} + R_{mix}}\right) \tag{23}$$

where

$$R_{mix} = \frac{1}{L_{mix} \cdot ER} \tag{24}$$

and

$$R_{crack} = \begin{cases} \left(R_{mix} - \dfrac{A_b}{Q_s}\right)\left(e^{-\xi} - 1\right) \ \ \Delta p \ > 0 & (25a) \\ \dfrac{L_{ck}}{D_g \cdot \eta} \ \ \Delta p = 0 & (25b) \end{cases}$$

with

$$\xi = \frac{Q_s}{A_b} \cdot \frac{L_{ck}}{D_g \cdot \eta} \tag{26}$$

where L_{mix} [L] is the enclosed space volume/infiltration area ratio, ER [$1/T$] the air building exchange, A_b [L^2] the foundation area in contact with soil, Δp [$M/L/T^2$] the pressure difference between the soil and the building, η [L^2/L^2] the foundation cracks fraction ($\eta = w_{ck} \cdot l_{ck}/A_b$), and Q_s [L^3/T] the convective flow rate from the soil into the building [*Johnson and Ettinger*, 1991; *Nazaroff*, 1988]:

$$Q_s = \frac{2\pi \cdot k_v \cdot \Delta p \cdot l_{ck}}{\mu \ ln\left(\frac{2d_f}{r_{ck}}\right)} \tag{27}$$

with

$$r_{ck} = \frac{\eta \cdot A_b}{l_{ck}} \tag{28}$$

where k_v [L^2] is the soil permeability to vapor flow, μ [L^2/T] the vapor viscosity, and l_{ck} [L] the foundation perimeter.

Alternatively, an empirical subslab-to-indoor air concentration attenuation factor, e.g., the generic attenuation factor based on the U.S. EPA's VI database [*U.S. EPA*, 2012], can be used to calculate indoor air concentration:

$$c_{in} = c_{ss} \cdot \alpha_{ss}^{in} \tag{29}$$

where α_{ss}^{in} is the empirical subslab-to-indoor air concentration attenuation factor, and c_{ss} represents the subslab concentration that can be either estimated from equation (18) by defining a specific position or, alternatively, can be conservatively set equal to the geometric mean of the horizontal subslab concentration profile along the whole subfoundation zone.

From equation (29), it is also possible to estimate the emission rate to indoor air, E_{in} [M/T], as follows [*Guo et al*., 2015]:

$$E_{in} = c_{in} \cdot V_b \cdot ER \tag{30}$$

where V_b [L^3] is the building volume.

3. Results and Discussions

3.1. Comparison With Field Data

Figure 2 shows a comparison between the results of the 2-D analytical model developed in this paper and the soil gas concentration of trichloroethylene (TCE) measured in a field experiment by *Holton et al*. [2013] and *Guo et al*. [2015] in three soil gas campaigns conducted under natural conditions. Located in Layton, UT, the field site is a split-level, two-story house with a slab-on-grade foundation footprint of 11.4 m $\times$ 7.4 m. The house overlies a regional dilute groundwater plume containing TCE. The groundwater was estimated to be 2.5 m below the foundation slab, and the average TCE concentration in groundwater was 24 μg/L. The soil between the ground surface and 0.6 m deep below surface was characterized as sand, and the soil from 0.6 m deep to the groundwater level was described as sandy clay. Readers interested in other details of the field site are directed to the original references.

This scenario was simulated with the developed model assuming the parameters reported in Table 1. The vapor source was assumed to be homogenous along the whole modeling domain and was calculated from the average TCE concentration in groundwater of 24 μg/L using the dimensionless Henry's constant (K_H) of TCE ($c_s = 24 \cdot 0.403 \cdot 10^3 = 9665\ \mu g/m^3$). The moisture content in the layer of sandy clay was calculated using the *van Genuchten* [1980] equation:

$$s_{ew} = \frac{\theta_w - \theta_r}{\theta_t - \theta_r} = \left(1 + (a \cdot H)^N\right)^{-M} \tag{31}$$

where s_{ew} is the dimensionless effective total fluid saturation, θ_w the soil water-filled porosity, a the point of inflection in the water retention curve [L^{-1}], θ_t the saturated soil water content, θ_r the residual soil water content, H the pressure head, [L], N the dimensionless van Genuchten curve shape parameter and M is equal to $1-1/N$.

The moisture content in the top layer was assumed to be that of sand in unsaturated zone from the EPA spreadsheet implementation of JEM [*U.S. EPA*, 2004].

The diffusion coefficient through the vadose zone was calculated with equation (11) assuming a vertical discretization of 0.005 m.

As to the data measured in the field, Figure 2 shows the soil gas concentration of TCE measured in the different multilevel (0.3 m b.g.s., 0.9 m b.g.s., and 1.8 m b.g.s.) sampling points (indicated by *Guo et al*. as 7, 1, E, and F) that were located beneath and adjacent to building foundations. Note that in Figure 2 the sampling points were represented in the building centerline considering the side view shown in legend of the figure.

From Figure 2, it can be observed that the developed model replicates with a reasonable approximation the soil gas concentration profile observed in the field, especially for the sampling point located beyond

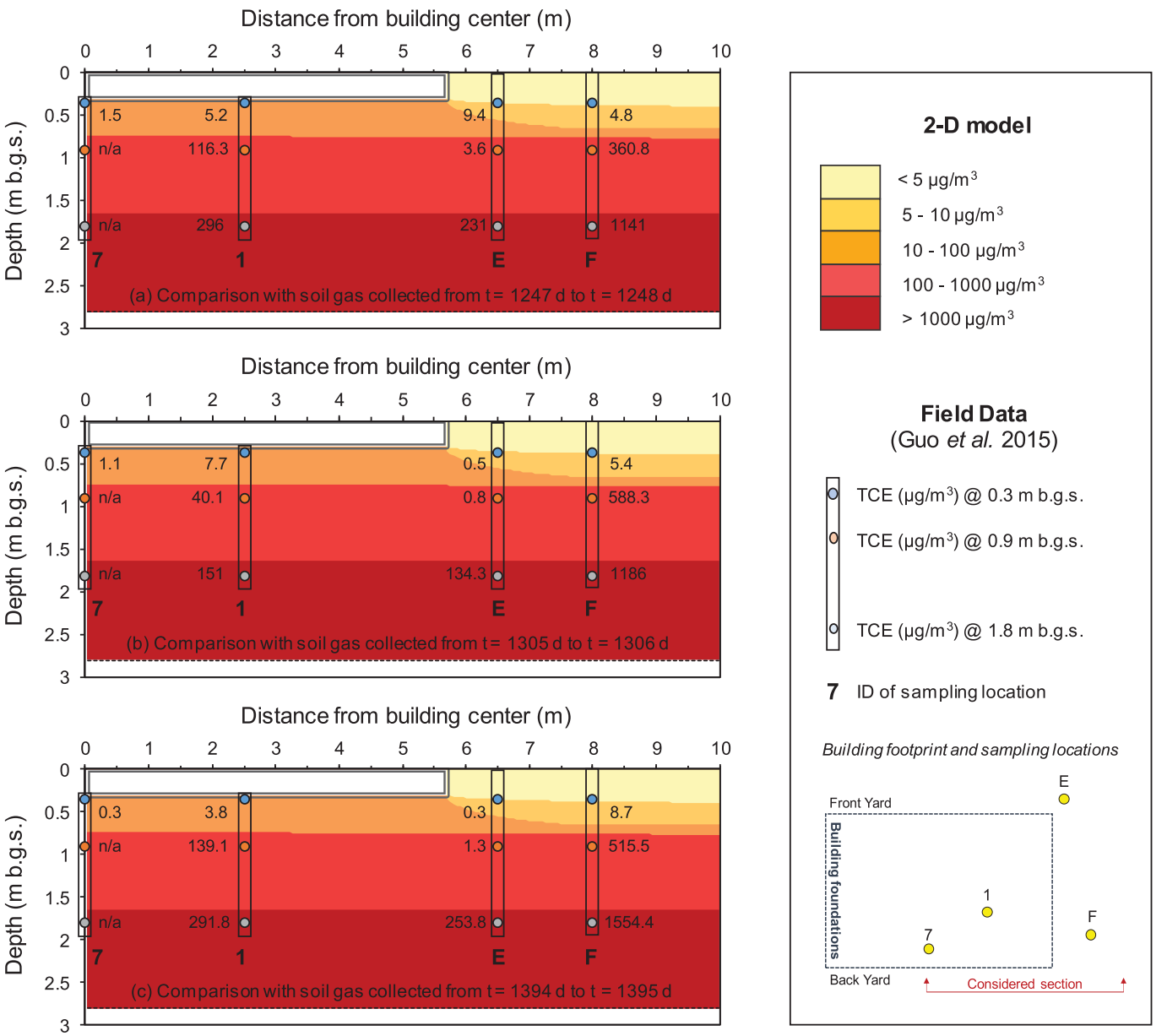

Figure 2. Comparison of soil gas concentration predicted by the developed model and the TCE concentrations measured by *Guo et al.* [2015] in three field campaigns carried out under natural conditions. The soil gas TCE concentration measured in the field is available in the supporting information of *Guo et al.* [2015].

the building foundations edge. In particular, it can be noticed that the soil-gas concentrations measured in the sampling point F always fall within the range expected by the model. By contrast, for the sampling points located beneath the building foundations, the profiles measured in the field differ by the ones expected by the model, with a general tendency of the latter to overestimate the soil gas concentrations. This latter result can be to some extent attributed to the effective location of sampling points with respect to building centerline but is most likely ascribed to the simplified assumption of homogenous source employed in the analytical model that not resembles the contamination scenarios observed in the field. Indeed, as showed by *Holton et al.* [2013] and *Guo et al.* [2015], the groundwater plume below the building is not uniform and this can explain the lower soil-gas concentration measured in some of the sampling points located beneath the building foundations.

Table 1. Input Parameters [*Abreu and Schuver*, 2012; *Holton et al.*, 2013; *Guo et al.*, 2015][a]

Parameter	Symbol	Unit	Figures 2 and 3	Figure 4	Figures 5 and 6
Indoor depressurization	Δ_p	Pa	1–3	5	5
Source depth from ground surface	d_s	m	2.8	8	4, 8
Foundation footprint length		m	11.4	10	10
Foundation footprint width		m	7.4	10	10
Foundation depth	d_f	m	0.3	2	0.2, 2
Volume of the enclosed space	V_b	m^3	177	174	366
Air exchange rate	A_e	h^{-1}	0.5	0.5	0.25
Foundation crack thickness	d_{ck}	m	0.1	0.15	0.15
Foundation crack width	w_{ck}	m	0.001	0.001	0.005
Henry's law constant	K_H		0.403	0.228	0.228
Soil gas permeability	k	m^2	1E-11 (sand)	1E-11 (high permeability) 1E-13 (low permeability)	Van Genuchten
Water-filled porosity	θ_w		0.054 (sand) Van Genuchten (sandy clay)	0.07 (high permeability) 0.21 (low permeability)	Van Genuchten
Total soil porosity	θ_t		0.35	0.35	Van Genuchten
Diffusion coefficient in air	D_g	m^2/s	6.87E-6	8.8E-6	8.8E-6
Diffusion coefficient in water	D_w	m^2/s	1.02E-9	9.8E-10	9.8E-10

Van Genuchten Parameters for the Different Soil Types

SCS soil name	a (m^{-1})	N	θ_t	θ_r	k (m^2)
Sand (S)	3.524	3.177	0.375	0.053	9.9E-12
Loamy sand (LS)	3.475	1.746	0.39	0.049	1.6E-12
Sandy loam (SL)	2.667	1.449	0.387	0.039	5.9E-13
Sandy clay loam (SCL)	2.109	1.33	0.384	0.063	2.0E-13
Loam (L)	1.112	1.472	0.399	0.061	1.9E-13
Silt loam (SiL)	0.506	1.663	0.439	0.065	2.8E-13
Clay loam (CL)	1.581	1.416	0.442	0.079	1.3E-13
Silty clay loam (SiCL)	0.839	1.521	0.482	0.09	1.7E-13
Silty clay (SiC)	1.622	1.321	0.481	0.111	1.5E-13
Silt (Si)	0.658	1.679	0.489	0.05	6.7E-13
Sandy clay (SC)	3.342	1.208	0.385	0.117	1.7E-13
Clay (C)	1.496	1.253	0.459	0.098	2.3E-13

[a]The Van Genuchten parameters for the different soil types are taken from *U.S. EPA* [2004].

For the same scenario described above, Figure 3 reports the TCE emission rates to indoor air measured by *Guo et al.* [2015] in the three field campaigns (using the "high-resolution-method," i.e., calculated for each of 20 soil gas snapshot sampling events) and the results obtained from equation (3) using the indoor concentration calculated by the 2-D analytical model with the classic "continuous stirred tank reactor" method (i.e., equations (23–28)). Making reference to this figure, it can be noticed that emission rates estimated from the field campaigns are very close to the ones expected by the model assuming a soil to building pressure difference between $\Delta p = 1$ Pa and $\Delta p = 3$ Pa (i.e., in the range of Δp measured by *Guo et al.* under natural condition). This latter comparison highlights that the screening model presented in this work can provide a reasonable estimate of the impact to indoor air expected from contaminated groundwater. It is worth mentioning that with respect to the modeling results obtained by *Guo et al.* [2015] using the EPA spreadsheet implementation of JEM, here we used the analytical model in a fully predicting way, i.e., by calculating

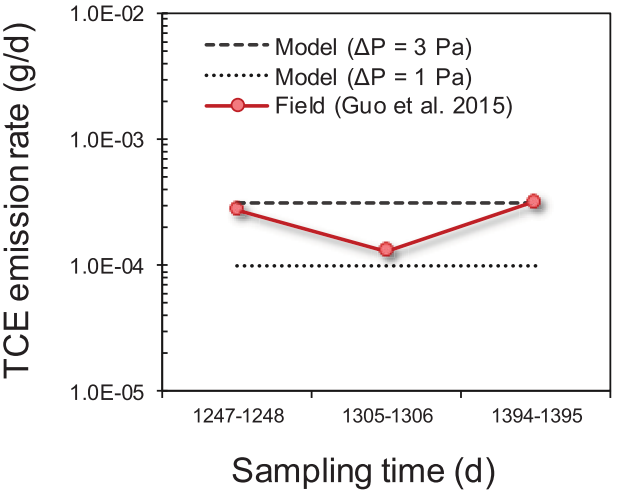

Figure 3. Comparison between the TCE emission rates to indoor air measured in the field by *Guo et al.* [2015] and the ones obtained using the 2-D model with assuming soil-building pressure difference between $\Delta p = 1$ Pa and $\Delta p = 3$ Pa. The TCE emission rates to indoor air refer to the "high-resolution method" data reported by *Guo et al.* [2015] in the supporting information.

the indoor emission rates from the average TCE groundwater concentration and by employing the *van Genuchten* [1980] and the *Millington and Quirk* [1961] equation for the estimation of the diffusion coefficient through the vadose zone.

3.2. Comparison With 3-D Simulations in Cases Involving Geological Barriers

Figure 4 shows a comparison between the 3-D simulated results in a U.S. EPA technical document by *Abreu and Schuver* [2012] and the predictions by the 2-D analytical model developed in this paper. These simulations were performed to study how laterally continuous soil layers can affect soil vapor concentration profile and indoor air concentration. The scenarios in Figure 4 represent a control system with uniform sandy soil, a four-layer system with two layers of higher moisture content below the building foundation, a six-layer system with two layers of higher moisture content beneath the foundation and a third layer on top of all, and a two-layer system with the higher moisture content layer on top. For the layers with the higher moisture content, the ratio of water-filled porosity to total porosity is 60% and the soil gas permeability is 10^{-13} m^2, while for the layers with the lower moisture content, the ratio of water-filled porosity to total porosity is 20% and the soil gas permeability is 10^{-11} m^2. In all the simulations, a homogenous source along the whole modeling domain was considered. Readers interested in other details are directed to the original EPA technical document [*Abreu and Schuver*, 2012].

This scenario was simulated with the developed model assuming the same parameters as used in the numerical model (see Table 1). Figure 4 shows that the predictions of the new model are in a good agreement with the numerical results, for both soil gas concentration profiles and for the source-to-indoor air attenuation factor (α). The relatively most significant difference of the soil gas concentration profiles lies in a small area around and above the building foundation corner. This is due to the fact that, in order to obtain an analytical solution, in the analytical model the concentration was assumed to be uniform at the level of foundation bottom beyond building edge. It is however worth mentioning that in practical applications this simplified assumption would not affect the general subslab soil gas concentration profiles, which are the focus of CVI site investigation. For the subslab concentration, the most significant difference is observed in the second scenario where the analytical model overestimates the attenuation by about 30% (e.g., at the building perimeter the analytical model estimates a normalized vapor concentration of around 0.15 against 0.2 predicted by the numerical model), while the maximum difference of α can be observed in the third scenario, where the prediction of the analytical model is about 2 times of the numerical result.

3.3. Comparison With 3-D Simulations in Cases Involving Groundwater Source

Figure 5 shows a comparison between the soil gas concentration profile and α obtained with a 3-D numerical model and those by the 2-D analytical model developed in this paper in the case of vertical moisture content variations. The full 3-D finite element model applied here was already presented in previous publications [*Pennell et al*., 2009; *Bozkurt et al*., 2009; *Yao et al*., 2011] and readers interested in more details are directed to the original references. The simulations were performed for a steady state scenario assuming nonbiodegradable contaminants in groundwater for a sand, sandy loam, and clay soil and two source depths (4 and 8 m). In both models, the *van Genuchten* [1980] equation (see equation (31)) was used to describe the vertical variation of soil moisture content.

The relative permeability for soil gas flow was calculated as reported by *Parker et al*. [1987]:

$$k_{r,g} = (1 - s_{ew})^{0.5} \left(1 - s_{ew}^{1/M}\right)^{2M} \tag{32}$$

where $k_{r,g}$ is the relative air permeability $\left(0 \le k_{r,g} \le 1\right)$.

The contaminant effective diffusion coefficient was calculated using the *Millington and Quirk* [1961] model shown in equation (9). In these simulations, we have again assumed a homogenous vapor source along the whole modeling domain. The parameter values used for these simulations are shown in Table 1.

From this comparison, it can be observed that also in the cases of vertical soil moisture content variations due to the capillary fringe effect, the results of the analytical model presented in this work are in a good agreement with the numerical simulations, for both soil gas concentration profiles and indoor air concentrations. Specifically, for the soil gas concentration profiles, the most significant difference is observed in the case of sandy loam soil and a source depth of 4 m. Here the analytical model overestimates the attenuation

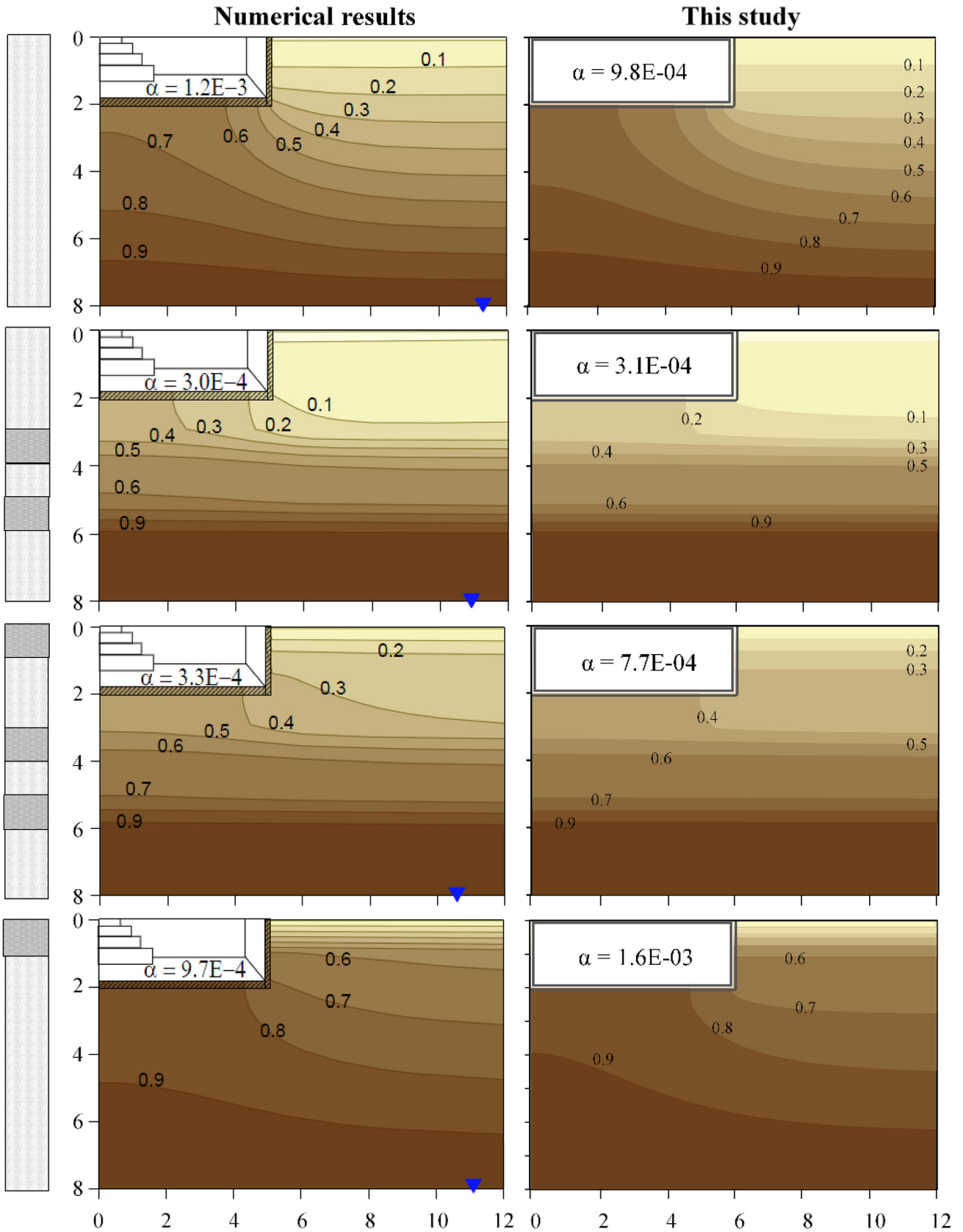

Figure 4. Comparison with the normalized vertical soil gas concentration profiles simulated by the 3-D numerical model for layering scenarios [*Abreu and Schuver*, 2012].

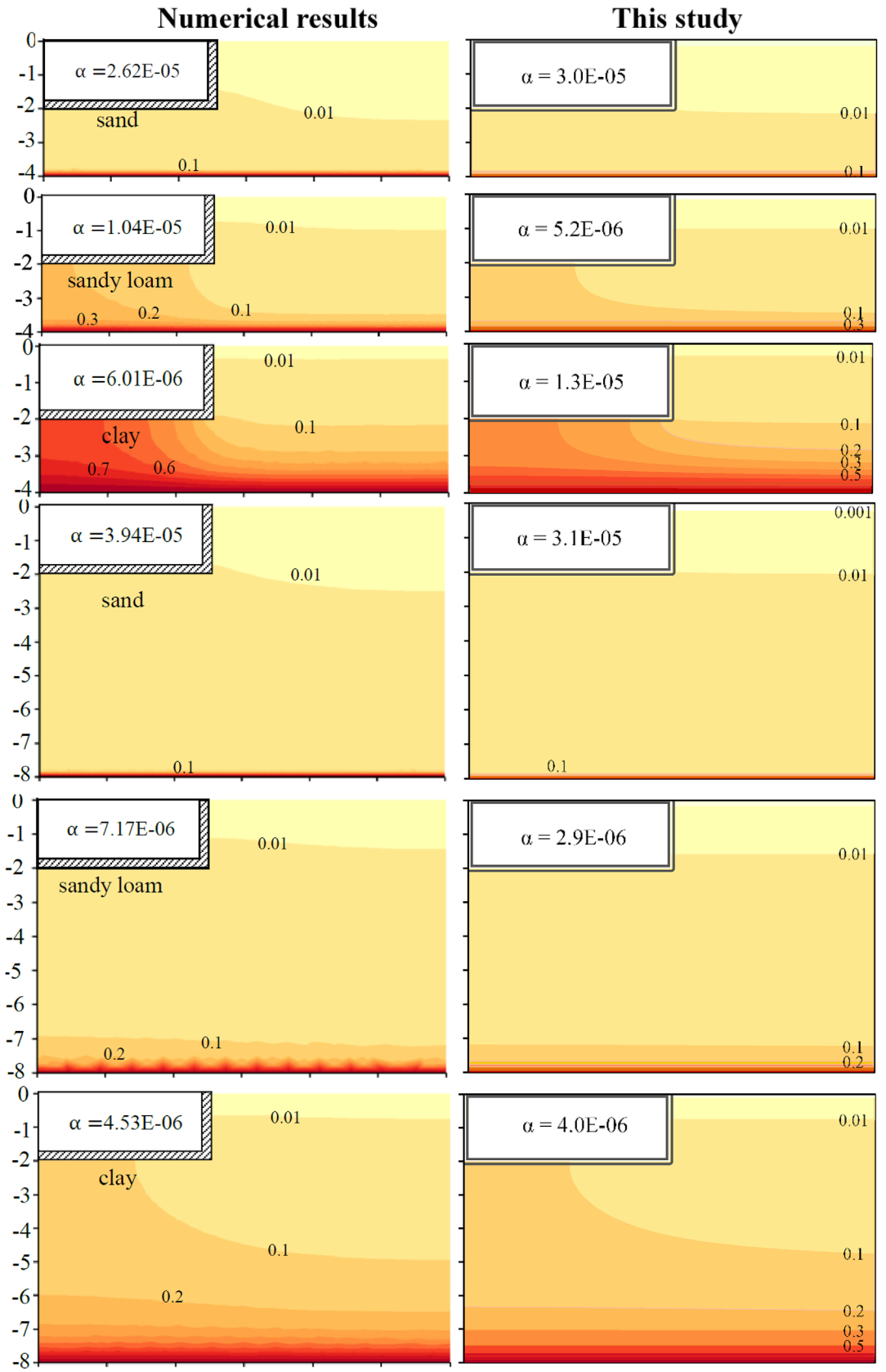

Figure 5. Comparison with the normalized vertical soil gas concentration profiles simulated by a 3-D numerical model for scenarios involving vertical soil moisture variations.

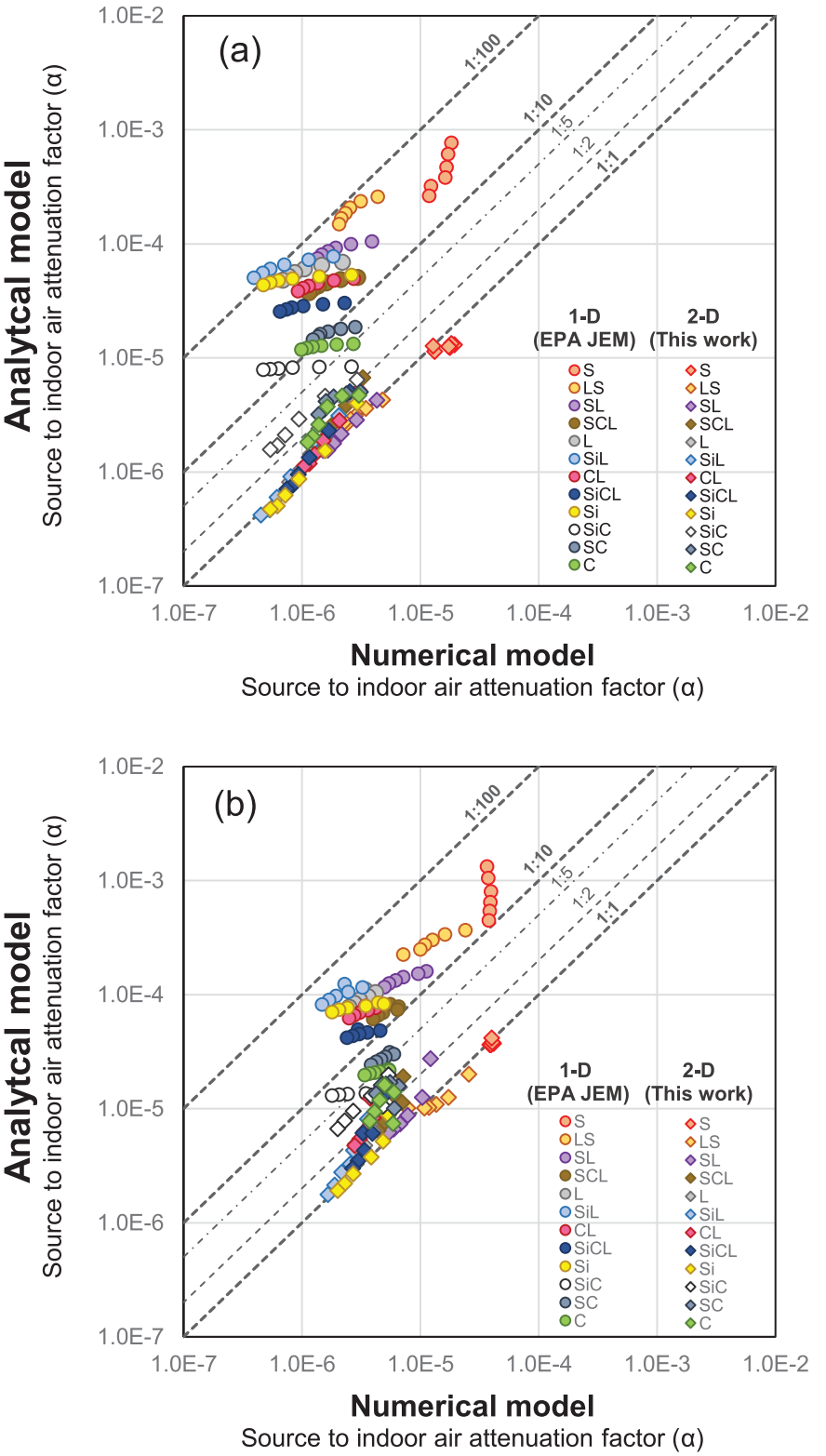

Figure 6. Comparison of source-to-indoor air attenuation factors for (a) slab-on-grade and (b) basement scenarios calculated with a 3-D numerical model and with the U.S. EPA Johnson and Ettinger model spreadsheet (EPA JEM, 1-D) and the model developed in this work for different types of soil. S = sand, LS = loamy sand, SL = sandy loam, SCL = sandy clay loam, L = loam, SiL = silt loam, CL = clay loam, SiCL = silty clay loam, Si = silt, SiC = silty clay, SC = sandy clay, C = clay.

by about 40%. The maximum difference of α can be observed in the second and third simulated scenario, although the variations are almost within a factor of 2.

3.4. Comparison With the U.S. EPA JEM Spreadsheet

Figure 6 reports a comparison of the source-to-indoor air attenuation factor (α) calculated with the 3-D numerical model described in the previous section and the results obtained using the simplified version of the JEM implemented in the U.S. EPA JEM spreadsheet [*U.S. EPA*, 2004] and the 2-D analytical model presented in this work. The calculated source-to-indoor air attenuation factors (α) used to generate Figure 6 are available in Supporting Information S1. It should be noted that the indoor air concentration was obtained using the classic "continuous stirred tank reactor" method (i.e., equations ((23–28))), in agreement with JEM. The simulations were performed in the case of homogenous groundwater source involving vertical moisture content variations in the case of different soil types and source depth for a slab-on-grade (Figure 6a) and basement scenario (Figure 6b). To describe the vertical variation of soil moisture content, the equation proposed by *van Genuchten* [1980] was used. The input parameters of these simulations are reported in Table 1. It is worth noting that in the simplified version of the JEM model implemented in the U.S. EPA spreadsheet, the vapor transport from groundwater through the soil overlying the source is approximated in two layers: a first layer describing the diffusion of vapors through the capillary fringe (characterized by a high moisture content) and a second layer describing the transport through the vadose zone. From the comparison shown in Figure 6b, it is evident that the two-layer approximation employed in the U.S. EPA JEM spreadsheet can lead to an overestimation of the indoor concentration up to two orders of magnitude compared to the numerical results. This is particularly emphasized in the cases of sandy soil as already elucidated by *Hers et al*. [2003] and *Shen et al*. [2012, 2013]. Considering that the two models share the same equation for the estimation of the subslab to indoor air attenuation factor, the different results observed in Figure 6 are attributed to an overestimation of U.S. EPA JEM spreadsheet in calculating the subslab crack concentration. By contrast, by employing an integral approach as suggested in the original model of *Johnson and Ettinger* [1991] and as implemented in the developed 2-D model (see equation (11)) we obtain results in good agreement with the numerical simulations with differences in nearly all cases within a factor of 2.

4. Conclusions

In this study, we presented a 2-D analytical model that can be used as a potential CVI risk screening tool, with a partial validation against field data and 3-D numerical results. As a 2-D model, it is capable of simulating lateral variation of subsurface soil gas concentration in layered soils involving homogenous sources, which cannot be done using the classic 1-D model. As an analytical model, it can be implemented in a spreadsheet for ease of use by practitioners and does not require extensive computation.

Moreover, in this new model we offer two methods for estimating indoor air contaminant concentrations. The first is the classic "continuous flow stirred-tank reactor" method as has been employed in JEM [*Johnson and Ettinger*, 1991; *U.S. EPA*, 2004] and AJM [*Abreu and Johnson*, 2005; *Abreu and Schuver*, 2012]. This method is generally used to calculate spatially and temporally averaged indoor air concentration, given a predicted entry rate of contaminant into the structure of concern. In this study, all calculations of indoor air concentration are based on this method, for the comparisons with JEM and AJM [*Johnson and Ettinger*, 1991; *Abreu and Schuver*, 2012].

The other method employs a predicted subslab concentration and an empirical subslab-to-indoor air concentration attenuation factor, which can be extrapolated from the U.S. EPA's VI database [*U.S. EPA*, 2012]. For instance, using the 95th percentile of the calculated attenuation factors in EPA's VI database, represents a conservative level of indoor air contaminant concentration for screening of residential buildings.

In the application of this model, readers must carefully evaluate its feasibility to the site of concern. Specifically, it should be considered that the proposed model is based on a typical CVI scenario of a single house overlying an infinite uniform vapor source and surrounded by open ground surface. Hence, practitioners should evaluate if these assumptions are reasonable for the investigated site. On the other hand, it should be noted that this new model does not include biodegradation, which limits its application as a risk screening tool for petroleum vapor intrusion. Finally, transient processes such as the temporal variation of moisture content due to events like rainfall or snow that can affect the vapor transport in the vadose zone [*Shen et al*., 2012; *Hers et al*., 2014] are ignored.

Acknowledgments
A spreadsheet implementation of this new model can be downloaded via www.pvitools.net. This work was funded in the part by the National Natural Science Foundation of China (21307108 and 21320102007) and National Institute of Environmental Health Sciences (P42ES013660).

References

Abreu, L. D. V., and P. C. Johnson (2005), Effect of vapor source-building separation and building construction on soil vapor intrusion as studied with a three-dimensional numerical model, *Environ. Sci. Technol.*, *39*(12), 4550–4561.

Abreu, L., and H. Schuver (2012), *Conceptual Model Scenarios for the Vapor Intrusion Pathway*, U.S. EPA, Washington, D. C.

Atteia, O., and P. Hohener (2010), Semianalytical model predicting transfer of volatile pollutant from groundwater to the soil surface, *Environ. Sci. Technol.*, *44*(16), 6228–6232.

Bozkurt, O., K. G. Pennell, and E. M. Suuberg (2009), Simulation of the vapor intrusion process for nonhomogeneous soils using a three-dimensional numerical model, *Ground Water Monit. Rem.*, *29*(1), 92–104.

Fischer, M. L., A. J. Bentley, K. A. Dunkin, A. T. Hodgson, W. W. Nazaroff, R. G. Sextro, and J. M. Daisey (1996), Factors affecting indoor air concentrations of volatile organic compounds at a site of subsurface gasoline contamination, *Environ. Sci. Technol.*, *30*(10), 2948–2957.

Guo, Y., C. Holton, H. Luo, P. Dahlen, K. Gorder, E. Dettenmaier, and P. C. Johnson (2015), Identification of alternative vapor intrusion pathways using controlled pressure testing, soil gas monitoring, and screening model calculations, *Environ. Sci. Technol.*, *49*(22), 13,472–13,482.

Hers, I., R. Zapf-Gilje, D. Evans, and L. Li (2002), Comparison, validation, and use of models for predicting indoor air quality from soil and groundwater contamination, *Soil Sediment Contam.*, *11*(4), 491–527.

Hers, I., R. Zapf-Gilje, P. C. Johnson, and L. Li (2003), Evaluation of the Johnson and Ettinger model for prediction of indoor air quality, *Ground Water Monit. Rem.*, *23*, 119–133.

Hers, I., P. Jourabchi, M. A. Lahvis, P. Dahlen, E. H. Luo, P. C. Johnson, G. E. DeVaull, and K. U. Mayer (2014), Evaluation of seasonal factors on petroleum hydrocarbon vapor biodegradation and intrusion potential in a cold climate, *Ground Water Monit. Rem.*, *34*(4), 60–78.

Holton, C., H. Luo, P. Dahlen, K. Gorder, E. Dettenmaier, and P. C. Johnson (2013), Temporal variability of indoor air concentrations under natural conditions in a house overlying a dilute chlorinated solvent groundwater plume, *Environ. Sci. Technol.*, *47*(23), 13,347–13,354.

Johnson, P. C., and R. A. Ettinger (1991), Heuristic model for predicting the intrusion rate of contaminant vapors into buildings, *Environ. Sci. Technol.*, *25*(8), 1445–1452.

Johnston, J. E., and J. M. Gibson (2013), Screening houses for vapor intrusion risks: A multiple regression analysis approach, *Environ. Sci. Technol.*, *47*(11), 5595–5602.

Man, J., W. Li, L. Zeng, and L. Wu (2016), Data assimilation for unsaturated flow models with restart adaptive probabilistic collocation based Kalman filter, *Adv. Water Resour.*, *92*, 258–270.

McHugh, T. E., L. Beckley, D. Bailey, K. Gorder, E. Dettenmaier, I. Rivera-Duarte, S. Brock, and I. C. MacGregor (2012), Evaluation of vapor intrusion using controlled building pressure, *Environ. Sci. Technol.*, *46*(9), 4792–4799.

Millington, R., and J. Quirk (1961), Permeability of porous solids, *Trans. Faraday Soc.*, *57*(10), 1200–1207.

Mills, W. B., S. Liu, M. C. Rigby, and D. Brenner (2007), Time-variable simulation of soil vapor intrusion into a building with a combined crawl space and basement, *Environ. Sci. Technol.*, *41*(14), 4993–5001.

Nazaroff, W. W. (1988), Predicting the rate of ^{222}Rn Entry from soil into basement of a dwelling due to pressure-driven air flow, *Radiat. Prot. Dosim.*, *24*, 199–202.

Olson, D., and R. L. Corsi (2002), Fate and transport of contaminants in indoor air. *Soil Sediment Contam.*, *11*(4), 583–601.

Parker, J. C., R. J. Lenhard, and T. Kuppusamy (1987), A parametric model for constitutive properties governing multiphase flow in porous media, *Water Resour. Res.*, *23*(4), 618–624.

Pennell, K. G., O. Bozkurt, and E. M. Suuberg (2009), Development and application of a three-dimensional finite element vapor intrusion model, *J. Air Waste Manage.*, *59*(4), 447–460.

Picone, S., J. Valstar, P. van Gaans, T. Grotenhuis, and H. Rijnaarts (2012), Sensitivity analysis on parameters and processes affecting vapor intrusion risk, *Environ. Toxicol. Chem.*, *31*(5), 1042–1052.

Provoost, J., L. Reijnders, F. Swartjes, J. Bronders, P. Seuntjens, and J. Lijzen (2009), Accuracy of seven vapour intrusion algorithms for VOC in groundwater, *J Soils Sediments*, *9*(1), 62–73.

Robinson, A. L., and R. G. Sextro (1997), Radon entry into buildings driven by atmospheric pressure fluctuations, *Environ. Sci. Technol.*, *31*(6), 1742−1748.

Shen, R., K. G. Pennell, and E. M. Suuberg (2012), A numerical investigation of vapor intrusion—The dynamic response of contaminant vapors to rainfall events, *Sci. Total Environ.*, *437*, 110–120.

Shen, R., K. G. Pennell, and E. M. Suuberg (2013), Influence of soil moisture on soil gas vapor concentration for vapor intrusion, *Environ. Eng. Sci.*, *30*(10), 628–637.

Shen, R., K. G. Pennell, and E. M. Suuberg (2014), Analytical modeling of the subsurface volatile organic vapor concentration in vapor intrusion, *Chemosphere*, *95*, 140–149.

Turczyowicz, L., and N. Robinson (2001), A model to derive soil criteria for benzene migrating from soil to dwelling interior in homes with crawl spaces, *Hum. Ecol. Risk Assess.*, *7*(2), 387–415.

U.S. EPA (2004), User's guide for evaluating subsurface vapor intrusion into buildings, prepared by Environmental Quality Management for USEPA Office of Emergency and Remedial Response.

U.S. EPA (2012), EPA's vapor intrusion database: Evaluation and characterization of attenuation factors for chlorinated volatile organic compounds and residential buildings, EPA 530-R-10–002, Off. of Solid Waste and Emergency Response, Washington, D. C.

U.S. EPA (2015), Technical guide for assessing and mitigating the vapor intrusion pathway from subsurface vapor source to indoor, *OSWER Publ. 9200.2–154*, Off. of Solid Waste and Emergency Response, Washington, D. C.

Van Genuchten, M. T. (1980), A closed-form equation for predicting the hydraulic conductivity of unsaturated soils. *Soil Sci. Soc. Am. J.*, *44*(5), 892–898.

Verginelli, I., Y. Yao, Y., Y. Wang, J. Ma, and E. M. Suuberg (2016), Estimating the oxygenated zone beneath building foundations for petroleum vapor intrusion assessment, *J. Hazard. Mater.*, *312*, 84–96.

Yao, Y., R. Shen, K. G. Pennell, and E. M. Suuberg (2011), Comparison of the Johnson-Ettinger vapor intrusion screening model predictions with full three-dimensional model results, *Environ. Sci. Technol.*, *45*(6), 2227–2235.

Yao, Y., K. G. Pennell, and E. M. Suuberg (2012), Estimation of contaminant subslab concentration in vapor intrusion, *J. Hazard. Mater.*, *231–232*, 10–17.

Yao, Y., I. Verginelli, and E. M. Suuberg (2016), A two-dimensional analytical model of petroleum vapor intrusion, *Water Resour. Res.*, *52*, 1528–1539, doi:10.1002/2015WR018320.

Yu, S., A. J. A. Unger, and B. Parker (2009), Simulating the fate and transport of TCE from groundwater to indoor Air, *J. Contam. Hydrol.*, *107*(3–4), 140–161.

Zhang, J., L. Zeng, C. Chen, D. Chen, and L. Wu (2015), Efficient Bayesian experimental design for contaminant source identification, *Water Resour. Res.*, *51*, 576–598, doi:10.1002/2014WR015740.